

Article

Adsorption of Amido Black 10B by Zinc Ferrite and Titanium Dioxide

Jinlin Yang ¹, Xingnan Huo ¹, Hanxin Xiao ¹, Zongyu Li ¹, Hengjun Li ² and Shaojian Ma ^{1,*}

¹ State Key Laboratory of Featured Metal Materials and Life-Cycle Safety for Composite Structures, MOE Key Laboratory of New Processing Technology for Nonferrous Metals, Guangxi Higher School Key Laboratory of Minerals Engineering and Materials, College of Resources, Environment and Materials, Guangxi University, Nanning 530004, China; jlyang523@126.com (J.Y.)

² College of Chemistry and Chemical Engineering, Guangxi University, Nanning 530004, China

* Correspondence: 1615391004@alu.gxu.edu.cn; Tel.: +86-131-5266-0958

Abstract: This study focuses on the comprehensive recycling and utilization of zinc ferrite, a by-product of wet zinc refining, for the treatment of azo dye wastewater. It explores the adsorption performance of various materials on Amido Black 10B and analyzes the factors that influence the adsorption process. Zinc ferrite derived from the by-products of wet zinc refining, zinc ferrite synthesized via calcination, and titanium dioxide prepared using the sol-gel method are utilized as adsorbents, specifically targeting Amido Black 10B. By adjusting factors such as calcination temperature, mixing ratio, initial pH, adsorbent dosage, adsorption time, initial concentration, and reaction temperature, the effects on the adsorption of Amido Black 10B are studied. Additionally, the performance of composite materials consisting of different crystalline forms of titanium dioxide and purified zinc ferrite is examined. Furthermore, the adsorption process of Amido Black 10B by purified zinc ferrite/titanium dioxide is analyzed in terms of kinetics and thermodynamics. The results show that titanium dioxide and purified zinc ferrite, prepared at temperatures of 300 °C to 550 °C, achieve over 90% removal efficiency when co-adsorbing Amido Black 10B. The best performance is observed at a ratio of 4:6 for purified zinc ferrite to titanium dioxide, with removal efficiency exceeding 80%. The second-order kinetic model fits the adsorption data well, and higher initial solution concentrations lead to decreased adsorption rates. The adsorption process of purified zinc ferrite/titanium dioxide on Amido Black 10B is spontaneous, exothermic, and reduces system disorder. Higher temperatures negatively impact the adsorption process.

Keywords: zinc ferrite; titanium dioxide; adsorption; amido black 10B



Citation: Yang, J.; Huo, X.; Xiao, H.; Li, Z.; Li, H.; Ma, S. Adsorption of Amido Black 10B by Zinc Ferrite and Titanium Dioxide. *Processes* **2023**, *11*, 2173. <https://doi.org/10.3390/pr11072173>

Academic Editors: Norman Toro, Roberto Parra, Henrik Saxen, Alessandro Navarra and Mostafa Y. Nassar

Received: 16 April 2023

Revised: 13 July 2023

Accepted: 19 July 2023

Published: 20 July 2023



Copyright: © 2023 by the authors. Licensee MDPI, Basel, Switzerland. This article is an open access article distributed under the terms and conditions of the Creative Commons Attribution (CC BY) license (<https://creativecommons.org/licenses/by/4.0/>).

1. Introduction

Azo dyes are among the most significant types of textile dyes due to their ease of dyeing and synthesis. They possess structural diversity, characterized by one or more azo bonds (-N=N-), with the azo bonds typically connecting aryl groups, forming complex aromatic compounds [1]. There are various types of azo dyes, each with distinct properties [2]. Improper treatment of azo dye wastewater can have adverse effects on the environment, leading to water quality deterioration and posing threats to human life and health [3]. Under anaerobic conditions, the decomposition of azo dyes produces highly toxic aromatic amines, exhibiting teratogenic, carcinogenic, and mutagenic effects [4]. In this study, we target the azo dye Amido Black 10B (AB10B), representative of typical azo dyes, with a molecular formula of C₂₂H₁₄N₆Na₂O₉S₂. Proper treatment of harmful substances in printing and dyeing wastewater is crucial before its discharge into the natural environment. To effectively treat azo dye wastewater, researchers have developed various methods, including physical, chemical, and biological approaches, as well as their combined treatment technologies [5–8]. Physical methods encompass adsorption, ion exchange, and membrane filtration [9–11]. Chemical methods involve chemical oxidation, Fenton reagent,

and photocatalytic oxidation [12–14]. Biological methods include anaerobic microorganisms, aerobic biological, and anaerobic-aerobic biological combinations [15,16]. Among these technologies, adsorption is widely used due to its broad availability of adsorbents and simple process flow. Nanoscale zinc ferrite, known for its large specific surface area, structural stability, strong adsorption capacity, and narrow band gap, has attracted considerable attention from researchers worldwide. Zinc ferrite has been extensively applied as an adsorbent and photocatalyst in water and wastewater treatment. For instance, Rania Ramadan et al. [17] investigated the synthesis of ZnFe_2O_4 NPs and their effects on the physical properties of PVDF/PVC blend systems. The addition of ZnFe_2O_4 NPs enhanced the crystallinity of the blend system and confirmed their incorporation. The removal efficiency of Cd (II) using PVDF/PVC/10% ZnFe_2O_4 reached approximately 50% at pH 6 after 60 min, and the adsorption mechanism and kinetics were studied. Amin et al. [18] discussed the synthesis of zinc ferrite nanopowders from steel-making wastes using the co-precipitation method and investigated their adsorption capacity for selenium species. The synthesized nanopowders exhibited good adsorption capacity for selenium ions in aqueous media, with the adsorption data fitting the Freundlich isotherm model. Titanium dioxide, a wide-bandgap semiconductor, exists in three crystal forms: anatase, rutile, and brookite [19,20]. It possesses high oxidation efficiency, is non-toxic, exhibits strong light stability, and has stable chemical properties that are environmentally friendly [21]. Therefore, titanium dioxide is widely employed in the photocatalytic degradation of organic compounds. Faisal Ali et al. [22] investigated the photocatalytic degradation of chlorobenzene in aqueous solutions using CQD-decorated Fe-doped TiO_2 immobilized in glass fibers (GF). The catalyst demonstrated the successful removal of chlorobenzene from the wastewater effluent. Xiaoyong Wu et al. [23] prepared Nd- and C-codoped TiO_2 samples, significantly enhancing their visible light absorption. The codoped samples exhibited coverage of ultraviolet light from 200 to 900 nm and the entire visible light range. In the treatment of dye wastewater, zinc ferrite and titanium dioxide are typically utilized as catalysts in photocatalytic reactions. However, the adsorption effects of zinc ferrite and titanium dioxide on dyes have rarely been studied individually, and there are no reports on their composite dyes. During the exploration of purified zinc ferrite applications, it was discovered that the physical mixture of purified zinc ferrite and titanium dioxide exhibited excellent adsorption performance for AB10B. Consequently, zinc ferrite, titanium dioxide, and their physical mixture were employed as adsorbents in this study. Various methods can be used to synthesize zinc ferrite, including the sol-gel method, chemical co-precipitation method, hydrothermal synthesis method, and high-temperature calcination method [24–26]. Furthermore, zinc ferrite can be obtained from industrial by-products to improve the utilization rate of zinc resources. In this study, we focused on the treatment of azo dye wastewater and the comprehensive recovery and utilization of zinc ferrite, a by-product of zinc hydrometallurgy. Purified zinc ferrite, zinc ferrite synthesized by the calcination method, and titanium dioxide prepared by the sol-gel method were utilized as adsorbents, targeting AB10B as the adsorbate. We investigated the effects of the physical mixture of titanium dioxide with purified zinc ferrite and synthetic zinc ferrite at different calcination temperatures on the adsorption of AB10B. Moreover, we examined the impacts of different mixture proportions, initial pH and concentration of the solution, adsorbent dosage, adsorption time, and reaction temperature on the adsorption of AB10B. Additionally, we discussed the absorption mechanisms of AB10B by the physical mixture of titanium dioxide with different crystal forms and purified zinc ferrite. The Langmuir and Freundlich isotherm models were employed to analyze the adsorption types and the quasi-first- and quasi-second-order kinetic equations were used to analyze the adsorbent's surface diffusion rate. Finally, the Van Hoff equation was applied to determine the relevant thermodynamic parameters. The results indicated that the adsorption process was determined to be exothermic or endothermic. This study provides a theoretical basis for subsequent sample preparation in industrial printing and dyeing wastewater treatment.

2. Methods

2.1. Preparation of Zinc Ferrite and Titanium Dioxide

2.1.1. Preparation of Purified Zinc Ferrite

The thermostatic water bath was turned on to achieve a temperature of 85 °C in the bath. 50 g of zinc calcine was weighed and placed in a 500 mL beaker. Then, 350 mL of sulfuric acid with a concentration of 120 g/L was added to the beaker. Subsequently, the beaker was transferred to the thermostatic water bath, and the stirring speed was set to 400 rpm. After leaching with stirring for 2 h, the beaker was removed and allowed to cool and settle. The supernatant was then removed, followed by filtration and washing until the filtrate reached a neutral pH. The filter cake was dried and ground, and the resulting sample was labeled as PZ.

The particle size distributions of purified zinc ferrite powder before and after grinding are shown in Figures 1 and 2 and Table 1.

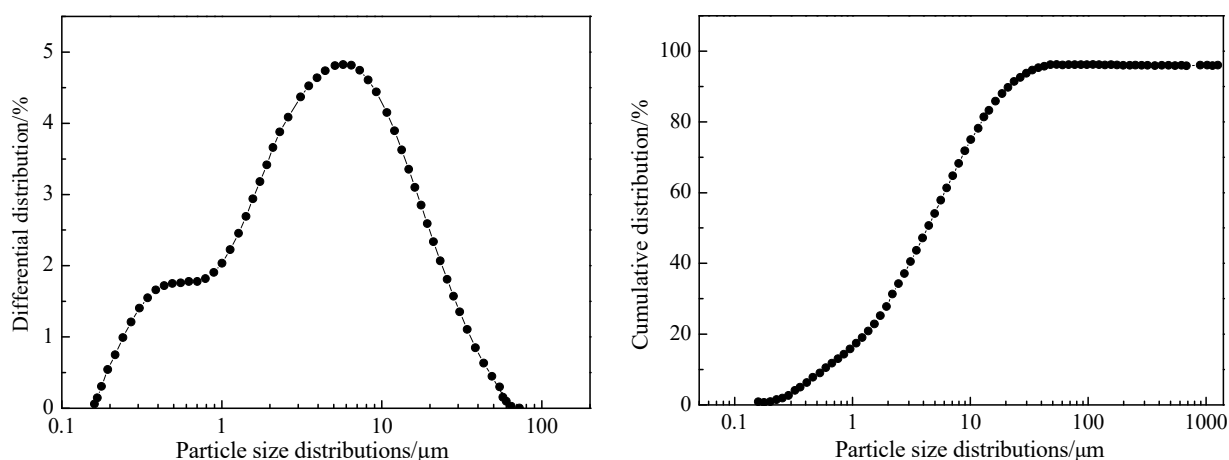


Figure 1. The particle size distribution of zinc ferrite samples before powdering.

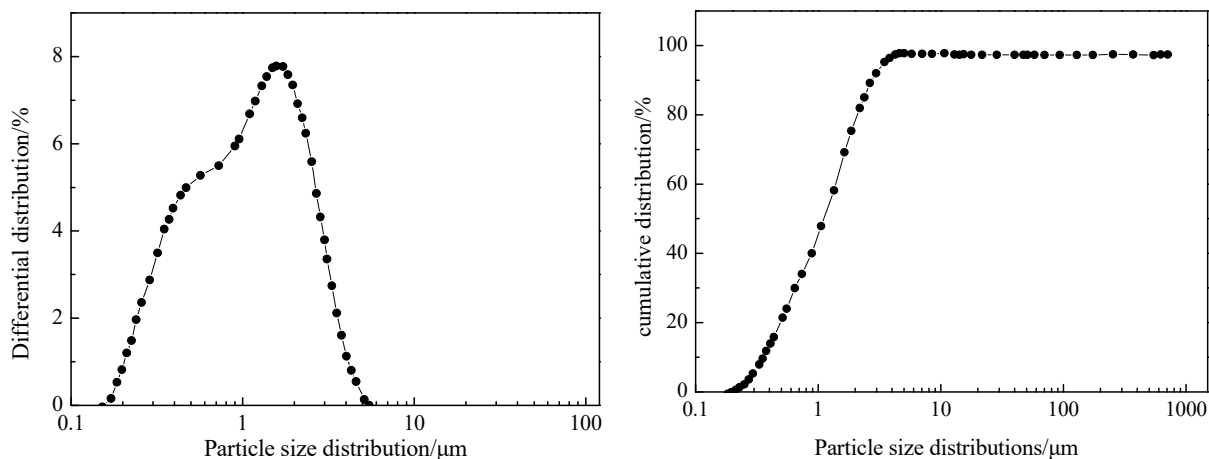


Figure 2. The particle size distribution of zinc ferrite samples after powdering.

As can be seen from Figures 1 and 2, the particle size distribution of purified zinc ferrite before grinding is as follows: within the particle size ranges of 0.158~1.096 μm , 1.096~10.000 μm , and 1.000~69.183 μm , the proportions are 17.59%, 57.73%, and 24.68%, respectively. The finer particle size range below 1.096 μm accounts for a smaller percentage. After grinding, the particle size distribution of purified zinc ferrite is as follows: within the particle size ranges of 0.158~1.096 μm and 1.096~5.754 μm , the proportions are 49.25% and 50.75%, respectively. The finer particle size range below 1.096 μm accounts for almost half of the entire particle size distribution. Additionally, the maximum particle size decreases from 69.183 μm to 5.754 μm , approximately a 12-fold reduction. Comparing Figures 1 and 2,

it can be observed that the particle size range of purified zinc ferrite after grinding is compressed towards the left.

Table 1. Adsorption isotherm model fitting parameters of AB10B adsorption on PZ/T400.

Temperature/°C	Langmuir Model			Freundlich Model		
	Q (mg/g)	K_L	R^2	K_F	1/n	R^2
15	31.538	4.341	0.932	22.187	0.221	0.935
25	42.864	3.231	0.995	28.873	0.280	0.936
35	40.579	2.775	0.963	26.401	0.267	0.899
45	39.489	2.125	0.917	24.093	0.283	0.889
55	37.054	1.935	0.882	22.256	0.271	0.864

2.1.2. Preparation of Synthetic Zinc Ferrite

A predetermined amount of ZnO and Fe₂O₃ was weighed according to the stoichiometric ratio of ZnFe₂O₄. The ZnO and Fe₂O₃ were mixed and then transferred into an oxidized zirconium grinding jar equipped with zirconia balls. The grinding jar was securely fixed, and the grinding machine was set to a rotation speed of 200 rpm. After mechanical activation for 3 h, the mixture of ZnO and Fe₂O₃ was transferred to a ceramic crucible. The crucible containing the ZnO and Fe₂O₃ mixture was placed in a high-temperature resistance furnace and subjected to calcination under an air atmosphere. The temperature was increased from 100 °C to 800 °C at a heating rate of 10 °C/min. After maintaining the temperature for 1.5 h, the calcined product was removed and allowed to cool. The cooled product was then ground, and the resulting sample was labeled as SZ.

2.1.3. Preparation of Titanium Dioxide

Different temperatures (300 °C, 350 °C, 400 °C, 450 °C, 500 °C, 550 °C, 600 °C) of titanium dioxide were prepared using the sol–gel method. For component A, a solution was prepared by mixing anhydrous ethanol, hydrochloric acid, and deionized water in a volume ratio of 25:0.5:1.0. For component B, a solution was prepared by mixing titanium butoxide and ethanol in a volume ratio of 10:12.5. The B solution was vigorously stirred using a magnetic stirrer, and the A solution was added to the B solution at a rate of one drop per second. After the complete addition of the A solution, the heating was turned on, and the temperature was raised to 40 °C. The heating and stirring were stopped when the mixture started forming a sol, and it was allowed to gel in the air. After aging for 6 h, the gel was dried at 105 °C for 12 h to obtain the precursor of titanium dioxide. The precursor was transferred to a ceramic crucible and placed in a high-temperature resistance furnace. The crucible was subjected to calcination under an air atmosphere. The temperature was increased from 100 °C to the desired temperature at a heating rate of 10 °C/min, and the crucible was maintained at the desired temperature for 2 h. After removal, the sample was naturally cooled in air and then ground using a vibration mill for 15 min. The resulting samples were labeled as T300, T350, T400, T450, T500, T550, and T600, respectively.

2.2. Adsorption Experiments

First, a standard solution of AB10B was prepared by weighing 4 g of AB10B powder and preparing a stock solution of 2 g/L of AB10B solution. According to the UV-visible absorption spectra of the AB10B solution, the absorption peak at 619 nm was the strongest. Therefore, the absorbance at 619 nm was used as the index to investigate the removal rate of AB10B in the solution. Using a pipette, an aliquot of the stock solution was dispensed and diluted to achieve a concentration of 200 mg/L. Subsequently, employing a sequential dilution approach, the solution was further diluted to establish a series of concentrations: 5 mg/L, 25 mg/L, 45 mg/L, 65 mg/L, 85 mg/L, 105 mg/L, and 125 mg/L. The prepared series of solutions were subsequently subjected to a 10-fold dilution. The absorbance of the resulting AB10B solutions at the wavelength of maximum absorbance (619 nm) was measured using a UV spectrophotometer. Finally, the standard curve of AB10B solution was

drawn, and the concentration of AB10B solution before and after treatment was calculated according to the standard curve in the follow-up test.

A certain amount of adsorbent was placed in a conical flask, and a certain volume of a concentration of C_0 AB10B solution was added each time. After sealing, the conical flask containing the adsorbent and solution was placed in a water bath with a constant temperature oscillator. After a certain period of oscillation, the flask was removed and filtered by a $0.45\ \mu\text{m}$ microporous filter membrane. Computed filtrate concentration C_t according to the formula. Two indexes, removal rate R and adsorption capacity q , were used to evaluate the adsorption effect of the adsorbent on the AB10B solution. The relevant calculation methods were shown in Formulas (1)–(3).

$$R = \frac{C_0 - C_t}{C_0} \times 100\%, \quad (1)$$

$$q_t = \frac{(C_0 - C_t) \times V}{m}, \quad (2)$$

$$q_e = \frac{(C_0 - C_t) \times V}{m}, \quad (3)$$

where C_0 is the concentration of AB10B solution in the solution before adsorption, mg/g; C_t is the concentration of AB10B solution in the solution at adsorption time t , mg/g; V is the volume of reaction solution, L; m is the mass of added adsorbent, g; q_e is the equilibrium adsorption capacity, mg/g; C_e is the concentration of AB10B solution in solution at adsorption equilibrium.

3. Results and Discussion

3.1. The Influencing Factors of Adsorption of AB10B by Zinc Ferrite and Titanium Dioxide

3.1.1. Effect of Physical Mixture of Purified Zinc Ferrite and Titanium Dioxide at Different Calcination Temperatures

The dosage of adsorbent was 2.0 g/L, and 0.05 g purified zinc ferrite and 0.05 g TiO_2 with different calcination temperatures were added to the conical flask. Under the conditions of solution pH 6.8, water bath temperature $25\ ^\circ\text{C}$, and oscillation speed 180 rpm, $0.45\ \mu\text{m}$ microporous filter membrane was used to filter the filtrate after 3 h adsorption, and the absorbance of the filtrate was measured. The removal rate and adsorption capacity of AB10B were calculated according to Formulas (2) and (3), respectively. The effect of the physical mixture of purified zinc ferrite and TiO_2 at different calcination temperatures on the adsorption of AB10B is shown in Figure 3.

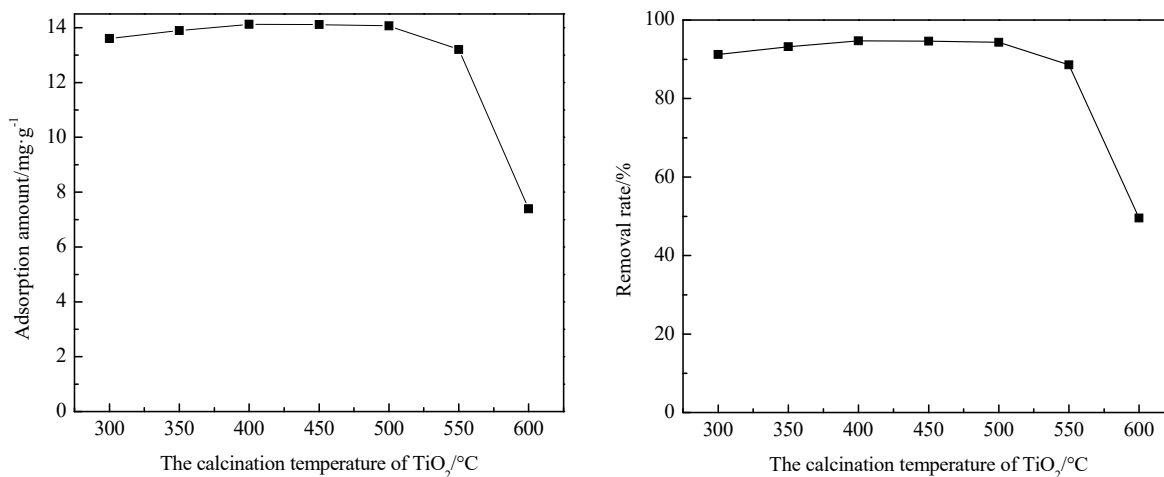


Figure 3. Effect of the calcination temperature of TiO_2 on adsorption capacity and removal rate of AB10B.

It can be seen from Figure 3 that in the range of calcination temperature from 300 °C to 400 °C, with the increase in calcination temperature of titanium dioxide, the adsorption amount and removal rate of AB10B gradually increased, but the increase rate is slow. In this temperature range, the crystallinity of titanium dioxide was relatively low but also had the characteristics of more surface defects, larger specific surface area, and more adsorption sites. The amount of AB10B on the surface of the adsorbent was more when it was fully contacted with AB10B. In addition, the adsorption capacity and removal rate of AB10B had no obvious change when the calcination temperature was 400 °C~450 °C. The reason may be that the crystals of titanium dioxide tend to be complete, and the reduction in surface defects. Additionally, when the calcination temperature was 550 °C, the adsorption capacity and removal rate of AB10B began to decrease. This may be caused by the decrease in surface defects and adsorption sites of titanium dioxide due to the increase in temperature. At 600 °C, the adsorption capacity and removal rate of AB10B decreased sharply. According to the analysis of XRD [27], titanium dioxide started to change from anatase type to rutile type at this temperature. The structure stability of rutile-type titanium dioxide was higher than that of anatase-type titanium dioxide, which also indirectly indicates that rutile-type titanium dioxide has fewer surface defects and fewer adsorption sites. According to the above analysis and energy consumption, TiO₂ calcined at 400 °C was used in the subsequent experiment.

3.1.2. Effect of Different Mixing Ratios of Zinc Ferrite and Titanium Dioxide

Weighed the sample according to the proportion of zinc ferrite (T400 = 9:1, 8:2, 7:3, 6:4, 5:5, 4:6, 3:7, 2:8, and 1:9), then mixed and added into the conical flask. Other conditions are the same as Section 3.1.1. The effects of different proportions of zinc ferrite and titanium dioxide AB10B on the adsorption capacity and removal rate of AB10B are shown in Figure 4.

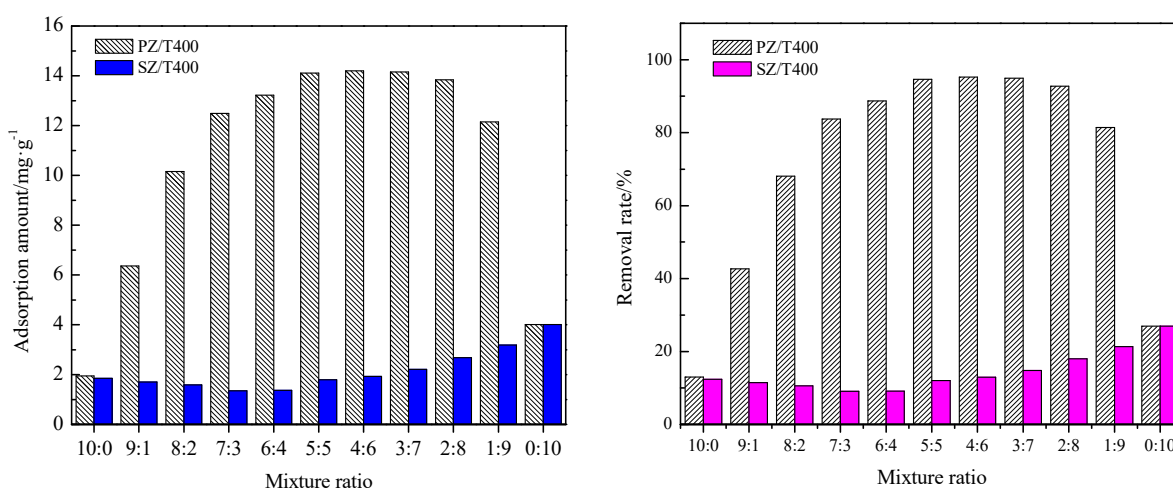


Figure 4. Effect of different proportions of zinc ferrites and titanium dioxide on the adsorption capacity and removal rate of AB10B.

According to Figure 4, the adsorption capacity and removal efficiency of AB10B show a consistent trend. The individual zinc ferrite (pure and synthesized) exhibits a removal efficiency of around 13% for AB10B, while the individual titanium dioxide shows a removal efficiency of around 26% for AB10B. This indicates that the standalone adsorption of AB10B by zinc ferrite or titanium dioxide alone is not effective.

However, when the proportion of titanium dioxide added is one-tenth, the adsorption performance of the mixed adsorbent of zinc ferrite and titanium dioxide rapidly improves to reach 42.67%. As the proportion of titanium dioxide in the zinc ferrite/titanium dioxide changes from 9:1 to 4:6, the removal efficiency and adsorption capacity of AB10B increase sharply and then plateau. Further increasing the proportion of titanium dioxide leads to a decrease in the removal efficiency and adsorption capacity of AB10B by the composite

material. When the proportion of zinc ferrite to titanium dioxide is 1:9, the removal efficiency of AB10B drops to 81.44%. In the case of the synthetic zinc ferrite/titanium dioxide, the removal efficiency and adsorption capacity of AB10B remain below 22% throughout the entire proportion range. Therefore, the optimal compositing ratio of zinc ferrite to titanium dioxide is determined to be 4:6. Consequently, this ratio will be used for subsequent experiments. To make a comparison with the synthetic zinc ferrite, the synthetic zinc ferrite/titanium dioxide will also be prepared using the same proportion.

3.1.3. Effect of Initial pH of AB10B Solution

The pH of the AB10B solution was 3, 5, 6.8, 9, and 11, respectively. 0.1 g of single or composite samples were weighed and added into conical bottles. Other conditions are the same as Section 3.1.1. The effect of the initial pH value of the solution on the adsorption capacity and removal rate of AB10B is shown in Figure 5.

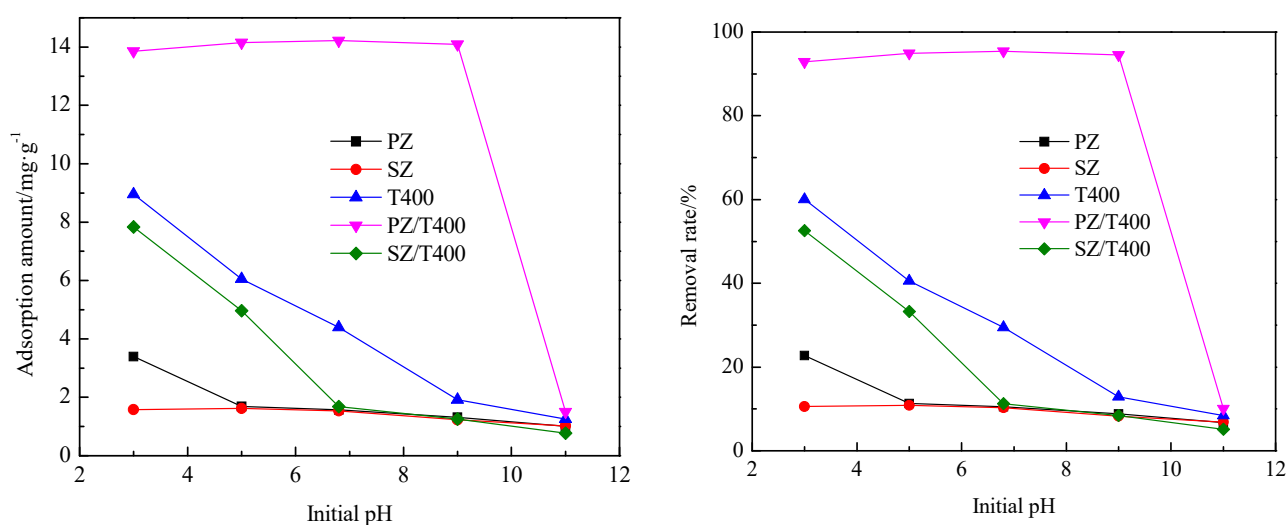


Figure 5. Effect of pH on the adsorption capacity and removal rate of AB10B.

It can be seen from Figure 5 that with the increase in pH of the solution, the adsorption capacity and removal rate of AB10B by purified zinc ferrite, synthetic zinc ferrite, titanium dioxide, and synthetic zinc ferrite/titanium dioxide decreased. The adsorption capacity and removal efficiency of purified zinc ferrite and titanium dioxide for AB10B did not change significantly in the range of pH 3~9, indicating that the composite of purified zinc ferrite/titanium dioxide has strong adaptability to the adsorption of AB10B when the solution is acidic or weakly alkaline. When pH = 3, the adsorption effect of several adsorbents on AB10B was better than that when the initial pH of the solution was greater than 3, except for the synthesis of zinc ferrite on AB10B was not good, and the adsorption effect of various adsorbents under acidic conditions was better than that under alkaline conditions. AB10B is a kind of anionic dye. When the acidity of the solution increases, the positive charge on the surface of zinc ferrite and titanium dioxide, the electrostatic attraction on the solid surface, and the electrostatic adsorption of AB10B increase due to the increase in H^+ in the solution, so the adsorption capacity is large. When the initial pH of the solution increased, the H^+ in the solution decreased, the OH^- increased, the negative charge on the surface of the adsorbent increased, and the electrostatic repulsion to AB10B increased. Thus, the adsorption capacity decreases. It was worth noting that the adsorption capacity of the purified zinc ferrite/titanium dioxide was still high at pH = 9, indicating that the adsorption effect of AB10B is better in the acidic and weak basic range in this adsorption system.

It can be seen from Figure 6 that the pH of the solution before and after the adsorption of AB10B by purified zinc ferrite, synthetic zinc ferrite, titanium dioxide, and synthetic zinc ferrite/titanium dioxide had little change, while the pH of the solution before and after the

adsorption of AB10B by purified zinc ferrite and titanium dioxide mixture decreased to varying degrees.

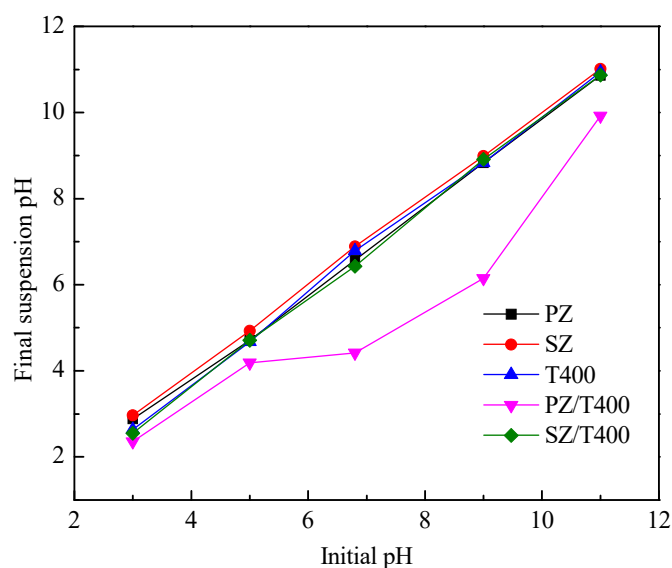


Figure 6. Changes of pH after AB10B adsorbed on various samples.

3.1.4. Effect of Dosage of Zinc Ferrite and Titanium Dioxide

Weighing 0.04 g, 0.06 g, 0.08 g, 0.10 g, 0.12 g, 0.14 g, and 0.16 g purified zinc ferrite, synthesized zinc ferrite, titanium dioxide, purified zinc ferrite/titanium dioxide, and synthetic zinc ferrite/titanium dioxide, respectively, and placed them in conical bottles. Other conditions are the same as Section 3.1.1. The effect of the amount of adsorbent on the adsorption capacity and removal rate of AB10B is shown in Figure 6.

It can be seen from Figure 7 that when the initial concentration of AB10B solution was 30 mg/L, the removal rate of AB10B in the solution was improved at a low dosage of purified zinc ferrite/titanium dioxide. When the dosage ranged from 0.12 g/L to 2.0 g/L, the removal rate increased slightly from 91.98% to 94.49%. However, with the increase in dosage, the removal rate was almost unchanged. It showed that the removal rate was almost unchanged, indicating that the removal rate of AB10B is not significantly increased with the increase in dosage of purified zinc ferrite and titanium dioxide mixed adsorbent. Correspondingly, the unit adsorption capacity of AB10B decreased from 22.86 mg/g to 8.77 mg/g, which decreased significantly. In addition, with the increase in titanium dioxide dosage, the removal rate of AB10B in the solution gradually increased, the removal rate of titanium dioxide for AB10B increased from 11.57% to 55.26%, and its unit adsorption capacity also increased gradually. However, the increased range was small, from 2.88 mg/g to 5.15 mg/g, indicating that with the increase in titanium dioxide dosage. With the increase in adsorption sites, the removal rate of a certain concentration of AB10B increases. Additionally, also found that, with the increase in the dosage of purified zinc ferrite, synthetic zinc ferrite, and synthetic zinc ferrite/titanium dioxide, the removal rate of AB10B increased slowly while the unit adsorption decreased gradually.

3.1.5. Effect of Adsorption Time

We weighed 0.10 g of purified zinc ferrite, synthetic zinc ferrite, titanium dioxide, purified zinc ferrite/titanium dioxide, and synthetic zinc ferrite/titanium dioxide, respectively, and placed them in conical bottles. Other conditions are the same as Section 3.1.1. The adsorption time was 10 min, 20 min, 30 min, 45 min, 60 min, 90 min, 120 min, 150 min, 180 min, 240 min, and 360 min, respectively. The effect of adsorption time on the adsorption capacity and removal rate of AB10B is shown in Figure 8.

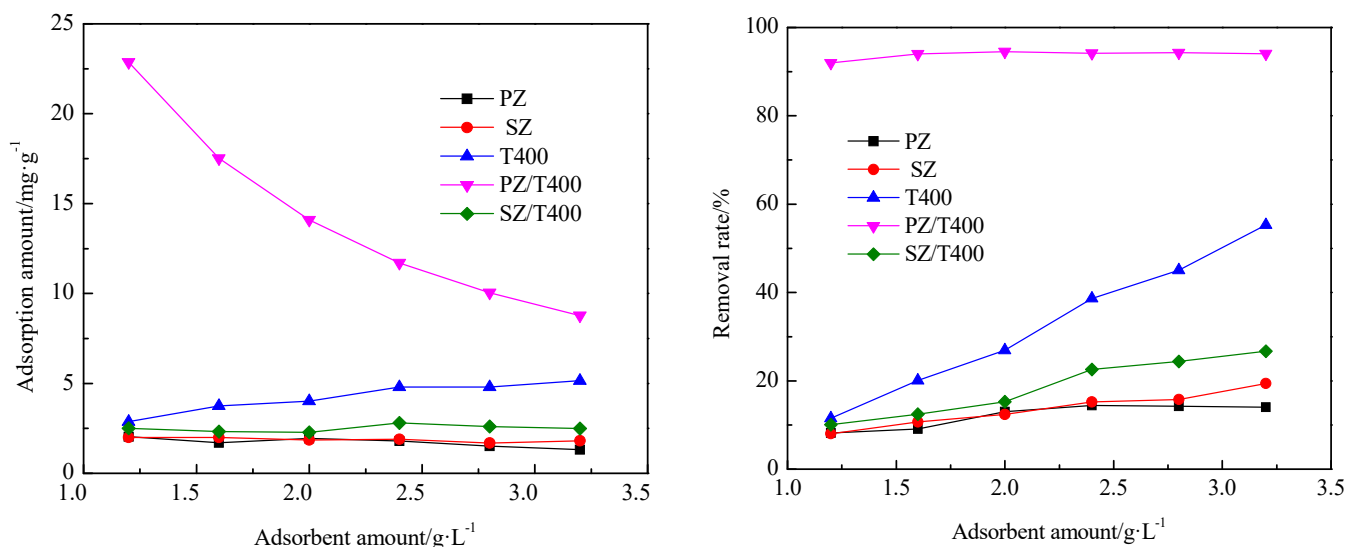


Figure 7. Effect of adsorbent dosage on the adsorption capacity and removal rate of AB10B.

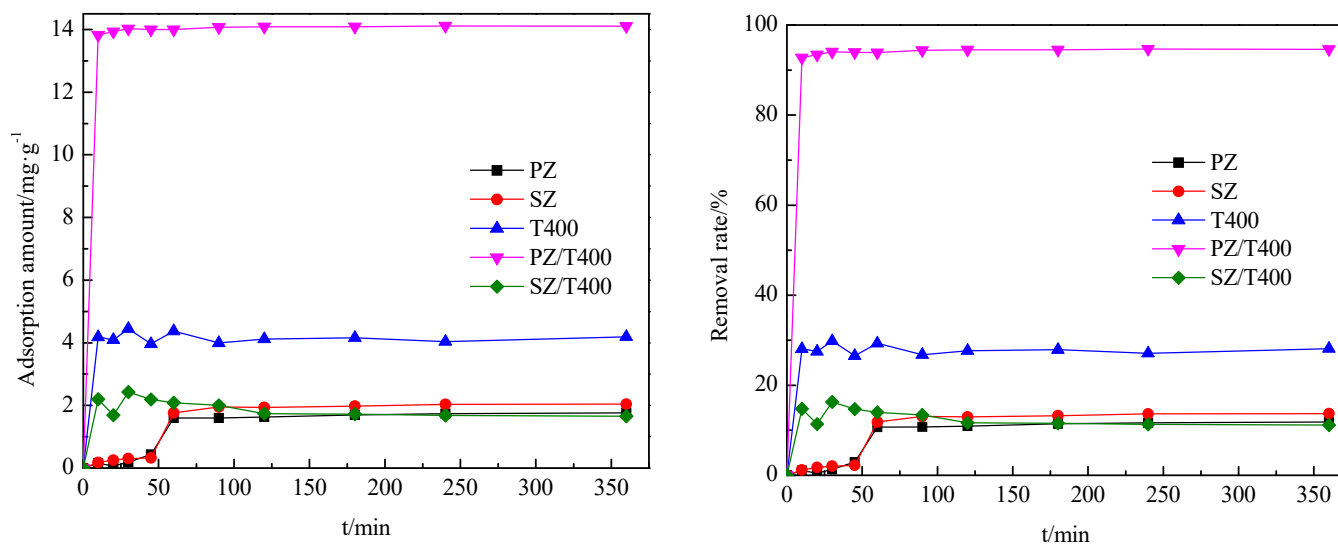


Figure 8. Effect of time on the adsorption capacity and removal rate of AB10B.

It can be seen from Figure 8 that the adsorption rate of purified zinc ferrite/titanium dioxide for AB10B was very fast, and it tended to reach equilibrium after 30 min, and the removal rate reached 94.06%. The other four adsorbents also reached adsorption equilibrium after 120 min, and the equilibrium adsorption capacity of titanium dioxide was relatively high, while the equilibrium adsorption capacity of purified zinc ferrite, synthetic zinc ferrite, and synthetic zinc ferrite/titanium dioxide was not significantly different.

3.1.6. Effect of Initial Concentration of AB10B Solution

We weighed 0.10 g of purified zinc ferrite, synthetic zinc ferrite, titanium dioxide, purified zinc ferrite/titanium dioxide, and synthetic zinc ferrite/titanium dioxide, respectively, in a conical bottle. The initial concentrations of AB10B solutions were 20 mg/L, 40 mg/L, 60 mg/L, 80 mg/L, 100 mg/L, and 120 mg/L, respectively. Other conditions are the same as Section 3.1.1. The effect of the initial concentration of the solution on the adsorption capacity and removal rate of AB10B is shown in Figure 9.

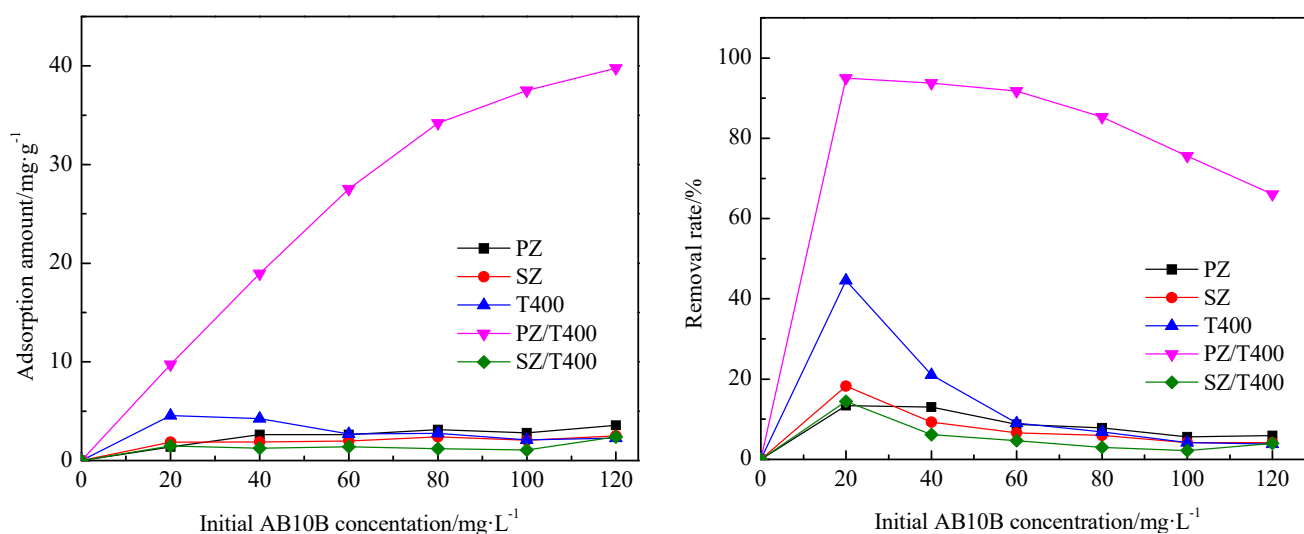


Figure 9. Effect of initial concentration of the solution on the adsorption capacity and removal rate of AB10B.

It can be seen from Figure 9 that the removal rate of AB10B decreased gradually with the increase in solution concentration of purified zinc ferrite, synthetic zinc ferrite, titanium dioxide, purified zinc ferrite/titanium dioxide, and synthetic zinc ferrite/titanium dioxide. However, the adsorption capacity of purified zinc ferrite, synthetic zinc ferrite, and synthetic zinc ferrite/titanium dioxide had no obvious change. Additionally, the adsorption capacity of AB10B by titanium dioxide decreased with the increase in initial solution concentration and then tended to be flat. It was worth noting that the adsorption capacity of purified zinc ferrite/titanium dioxide on AB10B increased with the increase in the initial concentration of the solution. In the initial concentration range of 20 mg/L~80 mg/L, the adsorption capacity of AB10B increased almost linearly. Additionally, in the initial concentration range of 80 mg/L~120 mg/L, the adsorption capacity of AB10B increased linearly. The adsorption capacity of AB10B began to slow down. When the initial concentration of the solution was 120 mg/L, the adsorption capacity of purified zinc ferrite/titanium dioxide on AB10B reached 39.75 mg/g, and the removal rate was 66.03%, indicating that purified zinc ferrite and titanium dioxide mixes adsorbent can treat relatively high concentration of AB10B dye wastewater.

3.1.7. Effect of Reaction Temperature

Weighed 0.10 g purified zinc ferrite/titanium dioxide into a conical flask and added AB10B solution with initial concentrations of 20 mg/L, 40 mg/L, 60 mg/L, 80 mg/L, 100 mg/L, and 120 mg/L. The water bath temperature was 15 °C, 25 °C, 35 °C, 45 °C, and 55 °C. The other conditions are the same as Section 3.1.1. The effect of reaction temperature on the adsorption of AB10B by purified zinc ferrite/titanium dioxide is shown in Figure 10.

It can be seen from Figure 10, in the range of 15 °C~55 °C, when the initial concentration of the solution was the same, with the increase in temperature, the adsorption amount and removal of purified zinc ferrite/titanium dioxide on AB10B first increased and then decreased. In the range of 25 °C~55 °C, when the initial concentration of the solution was 20 mg/L, the adsorption amount of AB10B decreased from 9.72 mg/g to 8.74 mg/g. When the initial solution concentration was 120 mg/L, the adsorption capacity of AB10B decreased from 39.75 mg/g to 32.38 mg/g. It can be seen that when the reaction temperature increased from 25 °C to 55 °C, the adsorption capacity of AB10B decreased slightly in the low-concentration region, while the adsorption capacity of AB10B decreased greatly in the high-concentration region. The reason may be that the AB10B molecules in the low-concentration region are mainly adsorbed on the surface sites of purified zinc ferrite and titanium dioxide, while some AB10B molecules in the high-concentration re-

gion have multilayer adsorption. With the increase in temperature, the energy of AB10B molecules increases, and the molecular thermal motion intensifies. Some AB10B molecules adsorbed on the solid surface overcome the electrostatic attraction and fall off from the solid surface. The molecular attraction of the outer layer of AB10B adsorbed in the high-concentration region is weak, and desorption occurs first. In addition, some of the AB10B molecules desorbed from the solid surface make the adsorption amount of AB10B in the high-concentration region decrease more significantly with the increase in temperature than in the low-concentration region. When the reaction temperature was 15 °C, the adsorption capacity of AB10B was lower in the initial solution concentration range of 60 mg/L~120 mg/L than that in the reaction temperature range of 25 °C~55 °C. It may be because the reaction temperature is too low, the molecular thermal motion is weakened, and some AB10B molecules cannot overcome the solid–liquid interface energy and cannot be adsorbed on the adsorbent.

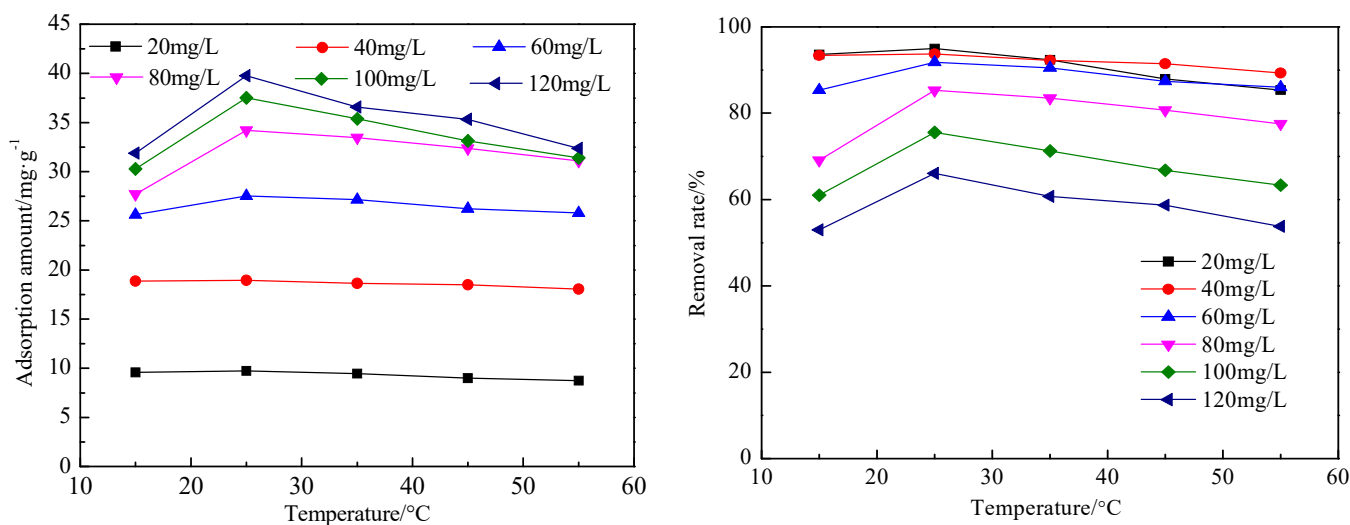


Figure 10. Effect of temperature on the adsorption capacity and removal rate of AB10B.

3.1.8. Adsorption of AB10B by Different Crystalline Titanium Dioxide Mixed with Purified Zinc Ferrite

To explore the difference between the properties of the self-made anatase titanium dioxide (T400) and the purchased anatase titanium dioxide (AT, 10 nm~25 nm) and titanium dioxide P25 (P25, 20 nm), 0.10 g of T400, PZ/T400, AT, PZ/AT, P25, and PZ/P25 were weighed, respectively and placed in a conical flask. Other conditions are the same as Section 3.1.1. The effect of purified zinc ferrite mixed with TiO₂ of different crystal types on the adsorption capacity of AB10B is shown in Figure 11.

According to Figure 11, the adsorption capacities of AT/PZ and T400/PZ are 14.14 mg·g⁻¹ and 14.20 mg·g⁻¹, respectively. When the AT/PZ and T400/PZ are used for the adsorption of AB10B, the adsorption capacities of the two composite materials for AB10B are comparable. The adsorption capacity of AT alone for AB10B is 1.5 mg·g⁻¹, while T400 alone has an adsorption capacity of 4.01 mg·g⁻¹ for AB10B. It can be concluded that the self-made anatase titanium dioxide exhibits better adsorption performance for AB10B compared to the purchased anatase titanium dioxide. This could be attributed to the lower crystallinity and higher surface defects of the self-made anatase titanium dioxide, leading to a higher exposure of Ti atoms on the surface and a positively charged solid particle surface, thereby increasing the adsorption capacity for AB10B. When P25, which consists of 80% rutile titanium dioxide and 20% anatase titanium dioxide, is mixed with purified zinc ferrite for the adsorption of AB10B, the adsorption capacity is only 0.66 mg·g⁻¹. This could be due to the presence of a large amount of rutile titanium dioxide in P25, which affects the adsorption performance of AB10B. The individual AT and T400 show unsatisfactory adsorption performance for AB10B. However, when mixed with purified zinc ferrite, the adsorption

capacity of AB10B increases by approximately $10 \text{ mg}\cdot\text{g}^{-1}$, indicating a synergistic effect between purified zinc ferrite and anatase titanium dioxide in the adsorption of AB10B.

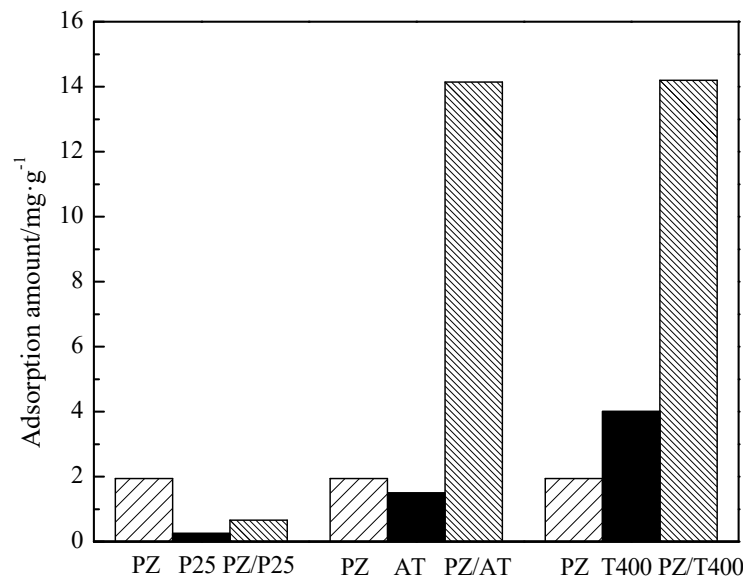


Figure 11. Effect of purified ZnFe_2O_4 mixed with different TiO_2 on the adsorption capacity of AB10B.

3.2. Model Building and Analysis

3.2.1. Adsorption Model of AB10B Mixed with Purified Zinc Ferrite and Titanium Dioxide

The Langmuir and Freundlich isothermal adsorption models are classical models for exploring the adsorption mechanism. Therefore, these two models were selected to fit the isothermal adsorption data, and the adsorption mechanism was analyzed according to the fitting data. The Langmuir isotherm adsorption model assumes that the adsorbate is attached to the surface of the adsorbent in a single layer, the adsorbent has the same adsorption site, the property is single, and the sites are independent of each other and are not affected by adjacent molecules, that is after the adsorbent site is occupied, the adsorbent will not be adsorbed. Langmuir isotherm is as follows:

$$q_e = \frac{QK_L C_e}{1 + K_L C_e} \quad (4)$$

where, q_e is the equilibrium adsorption capacity, mg/g ; Q is the adsorption capacity when the adsorbent reaches saturation, mg/g ; K_L is Langmuir adsorption equilibrium constant, C_e is the concentration of AB10B in solution at adsorption equilibrium. The correlation coefficient R^2 , the maximum adsorption capacity Q , and the equilibrium constant K_L of the fitting curve were obtained by plotting q_e versus C_e .

The Freundlich isothermal adsorption model is used to describe the multilayer heterogeneous adsorption process, and the interaction between adsorption sites is used to describe chemical adsorption. Freundlich isotherm is as follows:

$$q_e = K_F C_e^{1/n} \quad (5)$$

where q_e is the equilibrium adsorption capacity, mg/g ; C_e is the concentration of AB10B in solution at adsorption equilibrium. K_F is the Freundlich adsorption equilibrium constant. The larger the value of the heterogeneity coefficient n , the easier the adsorption. The correlation coefficient R^2 , equilibrium constant K_F , and heterogeneity coefficient n of the fitting curve are obtained by plotting q_e against C_e .

To investigate the isothermal adsorption model of purified zinc ferrite and titanium dioxide for AB10B, the adsorption data of purified zinc ferrite/titanium dioxide for AB10B were fitted using the Langmuir model (Equation (4)) and Freundlich model (Equation (5)),

respectively. The fitting curve is shown in Figure 12, and the relevant fitting parameters are shown in Table 1.

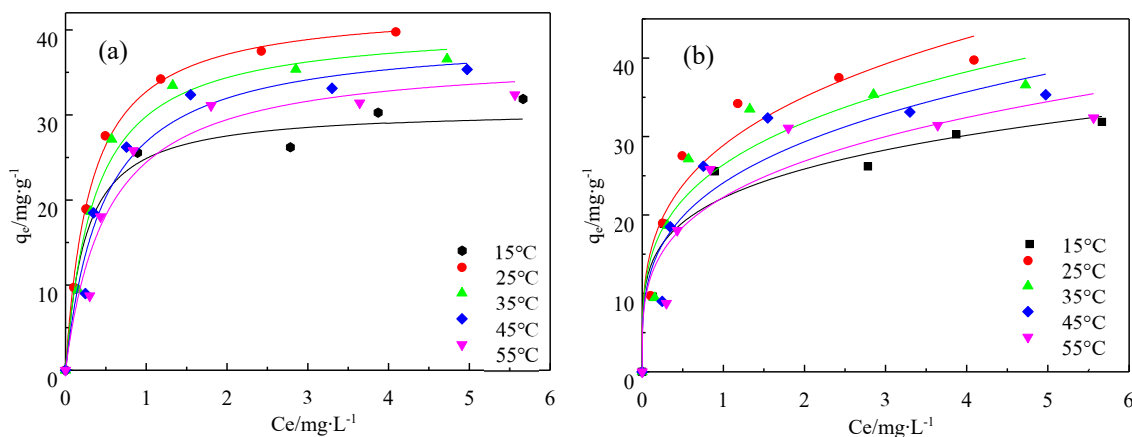


Figure 12. Isotherm of Langmuir (a) and Freundlich (b) for adsorption of AB10B on PZ/T400 at different temperatures.

Figure 12a,b, respectively, showed the adsorption isotherms of purified zinc ferrite/titanium dioxide on AB10B at different temperatures. It showed that the adsorption of purified zinc ferrite and titanium dioxide on AB10B was more consistent with the Langmuir model but deviated greatly from the Freundlich model. According to Langmuir adsorption theory, the surface of purified zinc ferrite and titanium dioxide had uniform adsorption capacity and a large number of atoms with residual valence force. It was speculated that the adsorption of purified zinc ferrite/titanium dioxide on AB10B was monolayer adsorption. Table 1 shows the maximum adsorption capacity Q of AB10B obtained by Langmuir model fitting was greater than the maximum adsorption capacity obtained in the experiment between 25 °C and 55 °C, showed that the adsorption of purified zinc ferrite and titanium dioxide on AB10B was not fully saturated. In the fitting parameters of the Freundlich model, the value of the adsorption index $1/n$ was less than 0.3, showing that the adsorption of AB10B on the purified zinc ferrite and titanium dioxide mixture was easier. It is consistent with the experimental results in 3.1.5.

3.2.2. Adsorption Kinetics of AB10B Mixed with Purified Zinc Ferrite and Titanium Dioxide

To explore the adsorption mechanism of composites on AB10B, a quasi-first-order kinetic model, and a quasi-second-order kinetic model were used to fit the experimental data. The quasi-first-order kinetic model is mainly used to investigate the adsorption efficiency of adsorbent and adsorbent, which is suitable for the external diffusion process of adsorbent on the surface of the adsorbent. The equation of the quasi-first-order dynamic model is:

$$\ln(q_e - q_t) = \ln q_e - k_1 t, \quad (6)$$

where q_e is the equilibrium adsorption capacity, mg/g; q_t is the adsorption capacity at time t , mg/g; t is time, min; k_1 is the adsorption rate constant. In the fitting calculation, the quasi-first-order dynamic equation can be used to fit the test data through its deformation, and q_t can be used to fit t . The equation is transformed into:

$$q_t = q_e (1 - e^{-k_1 t}), \quad (7)$$

The quasi-second-order dynamic equation is:

$$\frac{t}{q_t} = \frac{1}{k_2 q_e^2} + \frac{t}{q_e}, \quad (8)$$

where q_e is the equilibrium adsorption capacity, mg/g; q_t is the adsorption capacity at time t , mg/g; t is time, min; k_2 is the adsorption rate constant.

Figure 13a,b showed the quasi-first-order kinetic curve and quasi-second-order kinetic curve of purified zinc ferrite and titanium dioxide p-AB10B at different initial concentrations, respectively. The relevant fitting parameters are shown in Table 2.

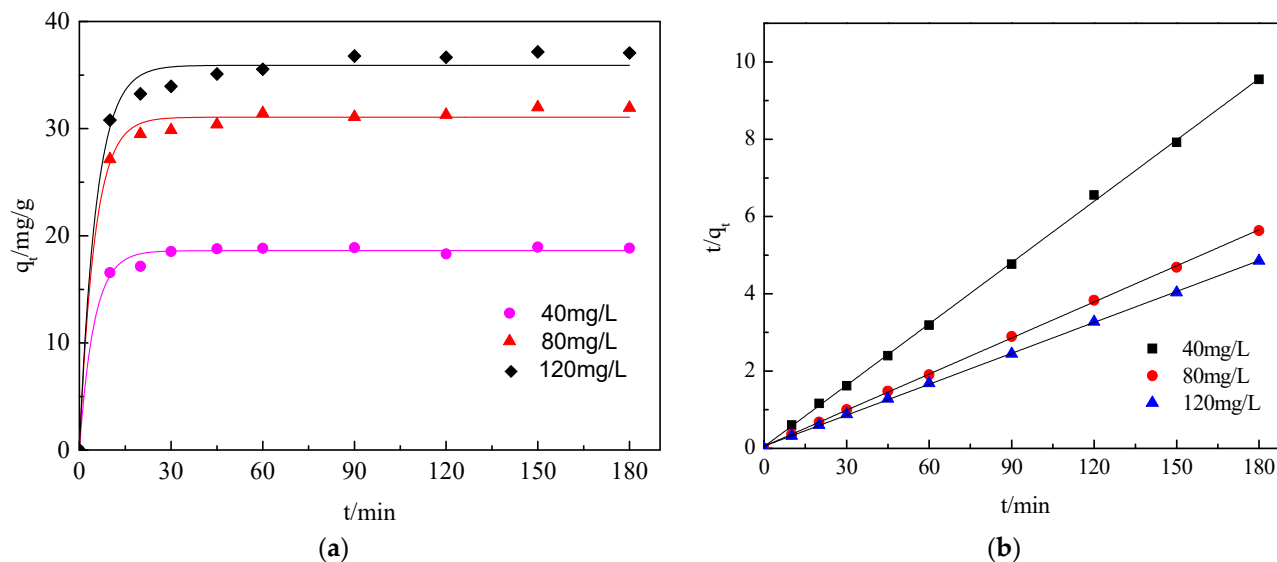


Figure 13. Fitting of adsorption kinetics by pseudo-first-order model (a) and pseudo-second-order model (b) for adsorption of AB10B on PZ/T400 at different initial concentrations.

Table 2. Kinetic model fitting parameters of AB10B adsorption on PZ/T400.

Initial Concentration/mg/L	Quasi-First-Order Dynamic Model			Quasi-Second-Order Dynamic Model		
	q_e (mg/g)	K_1	R^2	q_e (mg/g)	K_2	R^2
40	18.61	0.207	0.9932	18.90	0.060	0.9995
80	31.06	0.199	0.9940	32.12	0.018	0.9997
120	35.91	0.182	0.9886	37.49	0.012	0.9997

It can be seen from Figure 13 that the fitting effects of the two kinetic models were very good. With the increase in the initial concentration of the solution, the difference between the equilibrium adsorption capacity q_e obtained by pseudo-first-order kinetics fitting and the actual experimental value was larger. It can be seen from Table 2 that the correlation coefficient of fitting the obtained data with quasi-second-order kinetics was higher, R^2 was above 0.999, and the equilibrium adsorption capacity was equal to the actual test value. When the initial solution concentration increased from 40 mg/L to 80 mg/L, the adsorption rate constant K_2 decreased from 0.06 to 0.01, and the adsorption rate of AB10B on the surface of purified zinc ferrite and titanium dioxide was slowed down by increasing the concentration.

3.2.3. Adsorption Thermodynamics of AB10B Mixed with Purified Zinc Ferrite and Titanium Dioxide

To investigate the influence of temperature on the adsorption process and determine whether the adsorption of adsorbent on the adsorbent surface is an endothermic or exothermic reaction, the Gibbs-Helmholtz equation (Equation (9)) and not Hoff equations (Equation (10)) is used to solve the relevant thermodynamic parameters, namely Gibbs free energy ΔG , entropy change ΔS and enthalpy change ΔH . The equation is as follows:

$$\Delta G = -RT \ln K_L, \quad (9)$$

$$\ln K_L = \frac{\Delta S^\theta}{R} - \frac{\Delta H^\theta}{RT}, \quad (10)$$

where, R is the ideal gas constant, $R = 8.314 \text{ J}/(\text{mol}\cdot\text{K})$; T is the thermodynamic temperature, K ; K_L is the Langmuir adsorption equilibrium constant.

Figure 14 and Table 3, respectively, show the fitting line of $\ln K_L$ and $1/T$ and the relevant parameters obtained by fitting. Table 3 showed that Gibbs free energy ΔG^0 at all test temperatures was negative, indicating that the adsorption process can be spontaneous. The value of ΔG^0 increased from $-3.5154 \text{ kJ}\cdot\text{mol}^{-1}$ to $-0.7818 \text{ kJ}\cdot\text{mol}^{-1}$ with the increase in temperature, indicating that the adsorption of AB10B on the surface of purified zinc ferrite/titanium dioxide is not favorable with the increase in temperature, which verifies the conclusion that the adsorption reaction is not favorable with the increase in reaction temperature in Section 3.1.7. The negative value of ΔH^0 indicates that the adsorption process is exothermic, while the negative value of ΔS^0 indicates that the adsorption process is accompanied by a reduction in chaos, which is not conducive to spontaneous adsorption.

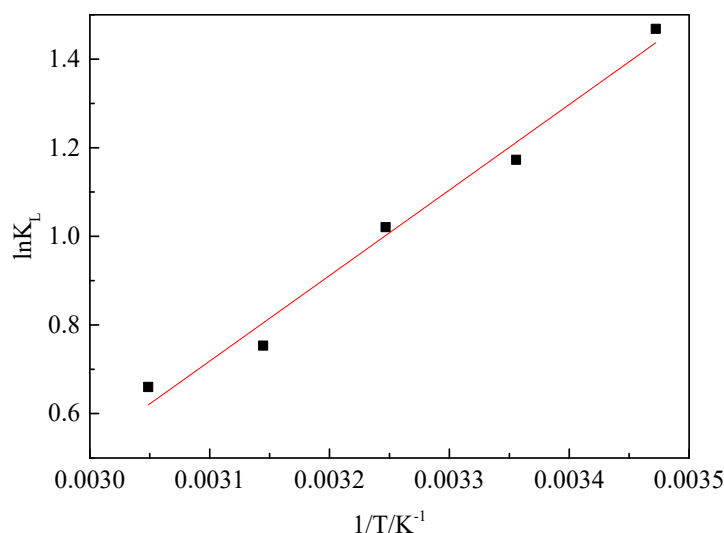


Figure 14. The relationship between $\ln K_L$ and $1/T$.

Table 3. Thermodynamic parameters for the adsorption of AB10B on PZ/T400.

Temperature/K	ΔG^0 (kJ·mol ⁻¹)	ΔH^0 (kJ·mol ⁻¹)	ΔS^0 (J·mol ⁻¹ ·K ⁻¹)
288	-3.5154		
298	-1.2620	-16.04	-43.76
308	-1.1349		
318	-0.8653		
328	-0.7818		

4. Conclusions

- (1) When the calcination temperature was 300 °C~550 °C, the titanium dioxide prepared was anatase type, and the removal rate of AB10B synergized with purified zinc ferrite was more than 90%. With the increase in calcination temperature, the removal rate of AB10B decreased, especially when the rutile phase appeared in anatase-type titanium dioxide. The removal rate of AB10B will drop sharply, which indicates that titanium dioxide crystal has a significant effect on the removal rate of AB10B. When the ratio of purified zinc ferrite to titanium dioxide mixture was 7:3~1:9, the removal rate of AB10B was above 80%, and the adsorption effect was the best when the ratio of zinc ferrite to titanium dioxide was 4:6. The initial pH of the solution, the initial concentration of the solution and the reaction temperature had significant effects on the adsorption capacity of AB10B, but the adsorption time had little effect.

- (2) The individual adsorption of AB10B by single purified zinc ferrite, single synthetic zinc ferrite, single titanium dioxide, and synthetic zinc ferrite/titanium dioxide exhibited lower removal rates compared to purified zinc ferrite/titanium dioxide. This indicates that the synergistic effect of purified zinc ferrite and titanium dioxide leads to enhanced adsorption performance. The adsorption capacity of AB10B using purchased anatase titanium dioxide and self-made anatase titanium dioxide, when mixed with purified zinc ferrite, showed similar results. However, the combination of titanium dioxide with the mixed crystal structure of anatase and rutile (P25) with purified zinc ferrite did not demonstrate a synergistic adsorption effect.
- (3) The adsorption behavior of purified zinc ferrite/titanium dioxide on AB10B followed the Langmuir isotherm model. The kinetics of the adsorption process indicated a better fit to the quasi-second-order kinetic model, and the adsorption rate decreased with increasing initial concentration of the solution. Thermodynamic analysis revealed that the adsorption process of purified zinc ferrite/titanium dioxide on AB10B was spontaneous, exothermic, and led to a decrease in system entropy. Furthermore, the adsorption process was found to be unfavorable with increasing temperature.

Author Contributions: Conceptualization, J.Y. and S.M.; Data curation, Z.L. and J.Y.; Formal analysis, H.L. and H.X.; Funding acquisition, J.Y.; Investigation, H.X. and J.Y.; Methodology, J.Y. and S.M.; Project administration, J.Y. and S.M.; Validation, X.H. and J.Y.; Writing—Original draft, X.H. and J.Y.; Writing—Review and editing, J.Y. and Z.L. All authors have read and agreed to the published version of the manuscript.

Funding: This research was funded by the National Natural Science Foundation of China (No. 52264020, No. 51774099).

Data Availability Statement: Not applicable.

Conflicts of Interest: The authors declare no conflict of interest.

References

1. Kong, F.; Wang, A.; Ren, H.Y. Improved azo dye decolorization in an advanced integrated system of bioelectrochemical module with surrounding electrode deployment and anaerobic sludge reactor. *Bioresour. Technol.* **2015**, *175*, 624–628. [[CrossRef](#)] [[PubMed](#)]
2. Fatima, M.; Farooq, R.; Lindström, R.W.; Saeed, M. A review on biocatalytic decomposition of azo dyes and electrons recovery. *J. Mol. Liquids* **2017**, *246*, 275–281. [[CrossRef](#)]
3. Chang, J.S.; Chen, B.Y.; Lin, Y.S. Stimulation of bacterial decolorization of an azo dye by extracellular metabolites from *Escherichia coli* strain NO₃. *Bioresour. Technol.* **2004**, *91*, 243–248. [[CrossRef](#)] [[PubMed](#)]
4. Ozyurt, M.; Ataçag, H. Biodegradation of azo dyes: A review. *Fresenius Environ. Bull.* **2003**, *12*, 1294–1302.
5. Ju, X.M.; Luo, L.T.; Zhang, H.T.; Huang, S.B.; Li, J.; Xiang, Y. Current situation and development trend of harmless treatment technology for dye wastewater in the fine chemical industry. *Sci. Technol. Rev.* **2021**, *39*, 45–54.
6. Cai, X.M.; Zheng, Y. Progress research on treatment technology of printing and dyeing wastewater. *Text. Auxilia.* **2018**, *35*, 5–8.
7. Holkar, C.R.; Jadhav, A.J.; Pinjari, D.V.; Mahamuni, N.M.; Pandit, A.B. A critical review on textile wastewater treatments: Possible approaches. *J. Environ. Manag.* **2016**, *182*, 351–366.
8. Wang, Z.; Xue, M.; Huang, K.; Liu, Z. Textile dyeing wastewater treatment. *Adv. Treat. Text. Effl.* **2011**, *5*, 91–116.
9. Yu, H.X.; Li, R.Y.; Liu, B.; Chen, X.; Yu, H.L. Printing and dyeing wastewater processing method. *Univ. Shanghai Sci. Technol.* **2017**, *39*, 320–322+333.
10. Greluk, M.; Hubicki, Z. Evaluation of polystyrene anion exchange resin for removal of reactive dyes from aqueous solutions. *Chem. Eng. Res. Des.* **2013**, *91*, 1343–1351. [[CrossRef](#)]
11. Mo, J.H.; Lee, Y.H.; Kim, J.; Jeong, J.Y.; Jegal, J. Treatment of dye aqueous solutions using nanofiltration polyamide composite membranes for the dye wastewater reuse. *Dye. Pigment.* **2008**, *76*, 429–434. [[CrossRef](#)]
12. Shi, Y.L.; Liang, Z.; Xiao, Y. Treatment of azo dye wastewater by the present research situation and progress. *Guangdong Chem. Industr.* **2012**, *39*, 140–141.
13. Ahmed, M.N.Z.; Chandrasekhar, K.B.; Jahagirdar, A.A.; Nagabushana, H.; Nagabushana, B.M. Photocatalytic activity of nanocrystalline ZnO, α -Fe₂O₃, and ZnFe₂O₄/ZnO. *Appl. Nanosci.* **2015**, *5*, 961–968. [[CrossRef](#)]
14. Li, L.G. Study on degradation of azo dyeing wastewater by photocatalysis oxidation of TiO₂. *J. Chem. Ind. Eng.* **2008**, *29*, 11–14.
15. Miao, Z.; Tao, J.; Li, S.; Wu, J.; Ding, Z.; Chen, X.; Ma, W.; Fan, H.J. Popcorn-like ZnFe₂O₄/CdS nanospheres for high-efficient photocatalyst degradation of rhodamine B. *Colloids Surf. A Physicochem. Eng. Asp.* **2022**, *654*, 130127.

16. Zhang, W.; Liu, F.; Wang, D.; Jin, Y. Impact of reactor configuration on treatment performance and microbial diversity in treating high-strength dyeing wastewater: Anaerobic flat-sheet ceramic membrane bioreactor versus up-flow anaerobic sludge blanket reactor. *Bioresour. Technol.* **2018**, *269*, 269–275. [[CrossRef](#)]
17. Amadan, R.; Ismail, A.M. Tuning the physical properties of PVDF/PVC/Zinc ferrite nanocomposites films for more efficient adsorption of Cd (II). *J. Inorg. Organomet. Polym. Mater.* **2022**, *32*, 984–998. [[CrossRef](#)]
18. Amin, A.M.; Rayan, D.A.; Ahmed, Y.M.; El-Shall, M.S.; Abdelbasir, S.M. Zinc ferrite nanoparticles from industrial waste for Se (IV) elimination from wastewater. *J. Environ. Manag.* **2022**, *312*, 114956. [[CrossRef](#)]
19. Cao, Y.; Li, X.; Bian, Z.; Fuhr, A.; Zhang, D.; Zhu, J. Highly photocatalytic activity of brookite/rutile TiO₂ nanocrystals with semi-embedded structure. *Appl. Catal. B Environ.* **2016**, *180*, 551–558. [[CrossRef](#)]
20. Liang, Y.; Huang, G.; Xin, X.; Yao, Y.; Li, Y.; Yin, J.; Li, X.; Wu, Y.; Gao, S. Black titanium dioxide nanomaterials for photocatalytic removal of pollutants: A review. *J. Mater. Sci. Technol.* **2022**, *112*, 239–262. [[CrossRef](#)]
21. Mahamud, M.; Tadesse, A.M.; Bogale, Y.; Bezu, Z. Zeolite supported CdS/TiO₂/CeO₂ composite: Synthesis, characterization and photocatalytic activity for methylene blue dye degradation. *Mater. Res. Bull.* **2023**, *161*, 112176. [[CrossRef](#)]
22. Ali, F.; Moin-Ud-Din, G.; Iqbal, M.; Nazir, A.; Altaf, I.; Alwadai, N.; Siddiqua, U.H.; Younas, U.; Ali, A.; Kausar, A.; et al. Ag and Zn doped TiO₂ nano-catalyst synthesis via a facile green route and their catalytic activity for the remediation of dyes. *J. Mater. Res. Technol.* **2023**, *23*, 3626–3637. [[CrossRef](#)]
23. Wu, X.; Yin, S.; Dong, Q.; Guo, C.; Kimura, T.; Matsushita, J.I.; Sato, T. properties of Nd and C codoped TiO₂ with the whole range of visible light absorption. *J. Phys. Chem. C* **2013**, *117*, 8345–8352. [[CrossRef](#)]
24. Masoudpanah, S.M.; Hasheminisari, M.; Ghasemi, A. Magnetic properties and photocatalytic activity of ZnFe₂-XLaXO₄ nanoparticles synthesized by sol-gel a method. *J. Sol-Gel Sci. Technol.* **2016**, *80*, 487–494. [[CrossRef](#)]
25. Ozcan, S.; Kaynar, B.; Can, M.M.; Firat, T. Synthesis of ZnFe₂O₄ from metallic zinc and iron by wet-milling process. *Mater. Sci. Eng. B* **2005**, *121*, 278–281. [[CrossRef](#)]
26. Botta, P.; Bercoff, P.; Aglietti, E.; Bertorello, H.; López, J.P. Synthesis and magnetic properties of zinc ferrite from mechanochemical and thermal treatments of Zn-Fe₃O₄ mixtures. *Mater. Sci. Eng. A.* **2003**, *360*, 146–152. [[CrossRef](#)]
27. Yang, J.; Huo, X.; Li, Z.; Ma, S. Study on preparation and properties of zinc ferrite and titanium dioxide. *E3S Web Conferen. EDP Sci.* **2023**, *385*, 4018. [[CrossRef](#)]

Disclaimer/Publisher's Note: The statements, opinions and data contained in all publications are solely those of the individual author(s) and contributor(s) and not of MDPI and/or the editor(s). MDPI and/or the editor(s) disclaim responsibility for any injury to people or property resulting from any ideas, methods, instructions or products referred to in the content.